Full text open access online (Since 2001)

PRINT: ISSN 0972-3757 ONLINE: ISSN 2456-6330
Int J Hum Genet, 26(2): 100-116 (2026)
DOI: 10.31901/24566330.2026/26.02.935

Chemo-Biological Evaluation and *In Vitro* Anticancer Effects of *Euphorbia hirta* on Lung Cancer Cells via *TP53*-Mediated Cell-Cycle and Proliferation Control

*Cuike Gong[1], Lei Qi[#], Juan He[3], Xiaolin Wang[4] and Aimin Li[*5]*

[1,3,4,5]The Second Department of Respiratory Medicine, Xingtai People's Hospital, Xingtai 054 000, China
[2]Department of Pathology, Xingtai People's Hospital, Xingtai 054 000 China

KEYWORDS *Euphorbia hirta*. Lung Cancer. Tumour Protein p53. Cell Cycle. Molecular Docking. Expression Analysis

ABSTRACT *Euphorbia hirta*, a medicinal plant rich in bioactive phytochemicals, was investigated for anti-lung cancer potential using integrated chemo-biological and in vitro assays in A549 cells. Phytochemicals from SuperTCM and IMPPAT were linked to lung cancer targets via SuperPred and GeneCards, and PPI analysis (STRING/Cytoscape) identified TP53, SRC, and EGFR as key hub genes enriched in MAPK, Akt, and HIF-1 pathways. Four major compounds (pinocembrin, naringenin, catechin, pelargonidin) collectively targeted 82 overlapping genes, while GEPIA2 confirmed elevated TP53 and EGFR expression in LUSC. *E. hirta* ethanolic extract showed dose-dependent cytotoxicity (IC50 = 35 µM), marked G0/G1 arrest, and significant TP53 downregulation by qRT-PCR at higher concentrations. Molecular docking revealed strong TP53 binding by naringenin. Overall, *E. hirta* demonstrates promising anti-lung cancer activity through TP53 modulation and oncogenic pathway inhibition, warranting further in vivo validation for therapeutic development.

INTRODUCTION

Lung cancer is a leading cause of cancer-related deaths globally, with approximately 2.2 million new cases and 1.8 million deaths annually, per recent WHO data (Li et al. 2023). High mortality stems from late diagnoses and limited treatments for advanced stages. Incidence is higher in developed nations due to historical smoking but is rising in developing regions from increasing tobacco use and environmental exposures. Key risk factors for lung cancer include smoking (approximately 85% of cases), secondhand smoke, occupational exposures (asbestos, radon), air pollution, genetics, chronic lung diseases, and diet (Thandra et al. 2021). It is classified into NSCLC (85%, including adeno-, squamous cell-, and large cell carcinoma with distinct molecular profiles) and the more aggressive SCLC. Advances like low-dose CT screening and precision medicine improve early detection and outcomes, but drug resistance and healthcare disparities remain challenges.

*Address for correspondence:
Dr. Aimin Li
E-mail: aiminli1@outlook.com
ORCID: 0009-0009-7189-0294
ORCID ID: 1st : 0009-0001-0328-549X
2nd: 0009-0007-7679-5670
3rd: 0009-0000-1556-3699
4th: 0009-0004-6994-973X

Unlike traditional pharmacology, which focuses on single-target mechanisms, network pharmacology maps multi-target, multi-pathway interactions, offering a holistic view of drug actions. In traditional Chinese medicine (TCM) and medicinal plant research, it has become indispensable for decoding the synergistic effects of herbal formulations (Jiashuo et al. 2022; Zhai et al. 2025). TCM's polyherbal remedies, which often involve multiple bioactive compounds, align well with network pharmacology's ability to analyse compound-target-disease networks. For instance, it helps identify active components in herbs, their molecular targets, and associated signalling pathways, facilitating the discovery of novel therapeutic agents. Applications include predicting drug efficacy, understanding mechanisms of action, and optimising herbal formulations for diseases like cancer, diabetes, and inflammation. By combining bioinformatics, omics data, and molecular docking, network pharmacology bridges TCM with modern medicine, enhancing drug development and personalised treatment strategies while validating the scientific basis of traditional remedies (Xin et al. 2021).

Euphorbia hirta, commonly known as asthma plant or snakeweed, is a widely distributed medicinal herb used in traditional medicine across tropical regions (Khursheed and Jain 2022). Its phytochemistry is rich and diverse, encompassing fla-

vonoids (for example quercetin, kaempferol), tannins, alkaloids, terpenoids, and phenolic compounds. These bioactive constituents contribute to its pharmacological properties, including anti-inflammatory, antioxidant, antimicrobial, anticancer, and anti-asthmatic activities (Tripathi et al. 2021; Iskandar et al. 2022). Studies have identified its potential in inhibiting cancer cell proliferation, particularly in lung and breast cancer, through mechanisms like apoptosis induction and cell cycle arrest (Widyananda et al. 2024). Its antimicrobial effects target pathogens like *Escherichia coli* and *Staphylococcus aureus*, while its anti-inflammatory properties are linked to the suppression of pro-inflammatory cytokines (Widyananda et al. 2024). In traditional medicine, *E. hirta* is used for respiratory disorders, wound healing and gastrointestinal issues. Recent research employs network pharmacology to map its bioactive compounds to molecular targets, revealing its therapeutic potential against complex diseases. However, challenges like toxicity at high doses and the need for standardised extracts underscore the importance of further studies to ensure safety and efficacy.

Objectives

This study aimed to explore the anticancer potential of *Euphorbia hirta* against lung cancer by investigating its bioactive compounds and their molecular mechanisms. A chemo-biological approach was employed to identify key targets, analyse compound-target interactions, and elucidate underlying pathways using bioinformatics and molecular docking, with the goal of discovering novel, cost-effective therapeutic candidates and supporting precision medicine strategies. Additionally, the study sought to validate the relevance of traditional medicinal use through modern scientific approaches.

MATERIAL AND METHODS

Phytochemical Identification

Phytochemicals present in *Euphorbia hirta* were identified using two comprehensive databases, that is, SuperTCM and IMPPAT. SuperTCM (http://tcm.mohualab.com/) serves as a detailed platform integrating chemical, biological, and pharmacological data for traditional Chinese medicine, providing extensive information on compound structures and bioactivities (Chen et al. 2025). IMPPAT (https://cb.imsc.res.in/imppat/) offers a curated resource of Indian medicinal plants, encompassing phytochemical structures, physicochemical properties, and therapeutic relevance (Vivek-Ananth et al. 2023). A thorough search of both databases yielded a list of bioactive compounds from *E. hirta*, focusing on those with documented pharmacological effects.

ADME and Toxicity Analysis

The pharmacokinetic behaviour of the identified phytochemicals was assessed using SwissADME (http://www.swissadme.ch/), a web-based tool that predicts absorption, distribution, metabolism, excretion (ADME) parameters, as well as drug-likeness and solubility profiles based on molecular descriptors (Daina et al. 2017). Parameters such as gastrointestinal absorption, blood-brain barrier permeability, and oral bioavailability were included. Toxicity profiling was carried out using ProTox-3.0 (https://tox-new.charite.de/protox3/), an advanced platform employing machine learning and structural similarity to forecast toxicological outcomes including hepatotoxicity, carcinogenicity, immunotoxicity, and mutagenicity.

Phytochemical Screening

To identify drug-like candidates, compounds were screened based on strict criteria, including oral bioavailability (OB) $\geq$ 30 percent, drug-likeness (DL) score $\geq$ 0.18, compliance with Lipinski's rule of five (molecular weight <500 Da, logP $\leq$ 5, hydrogen bond donors $\leq$ 5, acceptors $\leq$ 10), and molecular weight between 200-500 Da. Filtering through SwissADME's prediction algorithms led to the selection of four phytochemicals, namely, Pinocembrin, Naringenin, Catechin, and Pelargonidin. These compounds were chosen for further analysis based on their favourable ADME properties and potential pharmacological relevance.

Target Prediction

Target proteins for each selected phytochemical were predicted using the SuperTCM database. This platform combines chemoinformatic and bioinformatic tools to identify protein targets based

on molecular similarity, ligand-target interactions, and bioactivity data. For each compound, that is, Pinocembrin, Naringenin, Catechin, and Pelargonidin, high-confidence targets were identified using a probability threshold of ≥ 0.7 to ensure accuracy. These predicted targets were further examined for their association with lung cancer pathways, particularly those involved in oncogenesis and tumour suppression.

Lung Cancer-Related Targets

Lung cancer-associated genes were retrieved from the GeneCards database (https://www.genecards.org/), a robust bioinformatics resource providing gene annotations, expression profiles, and disease associations (Safran et al. 2022). To ensure relevance, only genes with a GeneCards Inferred Functionality Score (GIFtS) of ≥ 6 percent were included, emphasising their functional and pathological significance. The resulting gene set included major contributors to lung cancer such as EGFR, KRAS, and TP53. To determine the shared molecular targets between *E. hirta* phytochemicals and lung cancer, the gene lists from SuperTCM and GeneCards were compared using Venny 2.0 (https://bioinfogp.cnb.csic.es/tools/venny/).

PPI Network Generation

The common genes were submitted to the STRING database (version 11.5) (https://string-db.org/) for PPI analysis (Szklarczyk et al. 2025). Using a minimum interaction score of 0.7, the platform provided a high-confidence interaction network. The resulting data were imported into Cytoscape (v3.9.1), where the CytoHubba plugin was applied to calculate closeness centrality. This analysis identified the top 10 hub genes with the highest network connectivity, underscoring their potential as critical regulators in lung cancer biology.

GO and KEGG Pathway Analysis

Functional enrichment of the overlapping genes was conducted using ShinyGO (v0.77) (http://bioinformatics.sdstate.edu/go/), which integrates transcriptomic data for Gene Ontology (GO) and Kyoto Encyclopedia of Genes and Genomes (KEGG) pathway analysis (Ge et al. 2020). Significant enrichment was identified for biological processes, molecular functions, and cellular components, as well as key KEGG pathways. A false discovery rate (FDR) of < 0.05 was applied to maintain statistical rigour. The results were visualised using SRPlot (https://www.bioinformatics.com.cn/srplot), which provided publication-ready chord and bar plots for enriched pathways and gene interactions.

Differential Expression Analysis

Expression analysis of the top three hub genes was performed using GEPIA2 (http://gepia2.cancer-pku.cn/), a tool that merges RNA-seq data from The Cancer Genome Atlas (TCGA) and Genotype-Tissue Expression (GTEx) projects (Tang et al. 2019). Data from lung adenocarcinoma (LUAD) and lung squamous cell carcinoma (LUSC) cohorts were used to assess tumour versus normal tissue expression. Significant differences were evaluated using log, fold-change and p-values (< 0.05). In addition, Kaplan-Meier survival analysis was conducted to assess the prognostic value of these genes in lung cancer patients.

Molecular Docking

To explore potential molecular interactions, docking studies were conducted between TP53 and the selected phytochemicals. The 3D structure of TP53 (PDB ID: 4MZI) was retrieved from the RCSB Protein Data Bank (https://www.rcsb.org/) (Emamzadah et al. 2014). Ligand structures for Pinocembrin, Naringenin, Catechin, and Pelargonidin were sourced from PubChem (CIDs: 68071, 932, 9064 and 440832). Protein preparation involved removal of water molecules, ligands, and heteroatoms, and addition of polar hydrogens and Gasteiger charges using BIOVIA Discovery Studio. Ligands were energy-minimised using the MMFF94 force field. Docking was carried out using CB-Dock2 (http://cao.labshare.cn/cb-dock2/) (Liu et al. 2022), which predicts binding cavities and evaluates interactions. Docking outcomes included binding affinities (kcal/mol) and interaction types, which were visualised in 2D and 3D formats in Discovery Studio for comprehensive interpretation.

Chemicals, Reagents and Equipment

All chemicals and reagents used were of analytical grade and procured from Sigma-Aldrich. These included ethanol (Cat. No. E7023), DMSO

(D8418), MTT (M5655), PI (P4170), RNase A (R6513), DAPI (D9542), DMEM (D5796), FBS (F2442), Penicillin-Streptomycin (P4333), Trypsin-EDTA (T4049), and PBS (P4417). Major equipment used comprised a rotary evaporator (Rotavapor R-100, Buchi), centrifuge (Centrifuge 5810 R, Eppendorf), CO_2 incubator (Heracell 150i, Thermo Fisher), fluorescence microscope (Axio Observer Z1, Zeiss), microplate reader (Synergy H1, BioTek), and flow cytometer (FACS Aria III, BD Biosciences).

Extraction of *Euphorbia hirta* Aerial Parts

Aerial parts of *E. hirta* were collected, authenticated, and shade-dried at room temperature (25°C). The dried material (500 g) was pulverised into coarse powder and subjected to maceration in 2 litres of 95 percent ethanol for 72 hours. The mixture was filtered through Whatman No. 1 paper, and the filtrate was concentrated at 40°C under reduced pressure using a rotary evaporator. The concentrated extract was lyophilised to yield a dry residue, which was stored in an airtight container at 4°C until further use.

Preparation of Experimental Concentrations

A stock solution of 10 mg/mL was prepared by dissolving the dry extract in DMSO. Experimental concentrations (0, 15, 30, 60 and 120 μM) were obtained through serial dilution in DMEM supplemented with 10 percent FBS. The final DMSO concentration in each solution was maintained below 0.1 percent to avoid solvent-induced cytotoxicity. All working solutions were filter-sterilised using 0.22 μm syringe filters and stored at –20°C until use.

Cell Culture

Human lung adenocarcinoma A549 cells (ATCC CCL-185) were cultured in DMEM supplemented with 10 percent FBS and 1 percent Penicillin-Streptomycin. Cells were maintained at 37°C in a humidified atmosphere with 5 percent CO_2 . Subculturing was carried out using 0.25 percent Trypsin-EDTA upon reaching 80 to 90 percent confluence. Cell viability was assessed by trypan blue exclusion prior to experimental procedures.

MTT Assay

Cytotoxicity of *E. hirta* extract was determined via the MTT assay. A549 cells were seeded in 96-well plates at 5×10^3 cells/well and treated with varying concentrations of the extract for 48 hours. Post-treatment, 20 μL of MTT solution (5 mg/mL) was added to each well and incubated for 4 hours. Formazan crystals formed were dissolved in 100 μL of DMSO, and absorbance was measured at 570 nm using a microplate reader. Cell viability was expressed relative to untreated control, and $IC_{5.0}$ values were derived from dose-response curves.

Cell Cycle Assay

Cell cycle distribution was analysed using flow cytometry. A549 cells were treated with 0, 30, 60, and 120 μM extract for 48 hours. Post-treatment, cells were fixed in 70 percent ethanol and stored at –20°C overnight. Fixed cells were washed with PBS, incubated with RNase A (100 μg/mL) at 37°C for 30 minutes, and stained with PI (50 μg/mL) for 15 minutes in the dark. Flow cytometry was performed using a FACS Aria III system, and FlowJo software was used for cell cycle phase quantification.

mRNA Expression Analysis

Total RNA was extracted using TRIzol Reagent from A549 cells treated with 0, 30, 60, and 120 μM extract. RNA was purified through phase separation and alcohol precipitation, followed by verification of purity using a NanoDrop spectrophotometer. One microgram of RNA was reverse-transcribed using the iScript cDNA Synthesis Kit, and qRT-PCR was carried out with SYBR Green Master Mix. Primers specific to the gene of interest and GAPDH (internal control) were used. Amplification was done on a QuantStudio 3 system, and specificity was confirmed by melting curve analysis. Relative gene expression was determined using the $2^{-\Delta\Delta Ct}$ method, normalised to GAPDH and control samples.

Statistical Analysis

Data were expressed as mean ± SD (n = 3). Statistical significance was determined using one-way ANOVA followed by Tukey's test ($^{*}p < 0.05$, $^{**}p < 0.01$, $^{***}p < 0.001$).

RESULTS

Phytochemical Identification and Screening

A total of 78 and 129 phytochemicals from *Euphorbia hirta* were identified using the SuperTCM

and IMPPAT databases, respectively. After screening based on primary criteria (oral bioavailability ≥30%, drug-likeness score ≥0.18, Lipinski's rule, and molecular weight 200-500 Da), only four phytochemicals survived, namely, Pinocembrin, Naringenin, Catechin, and Pelargonidin. Their properties are summarised in Table 1, including canonical SMILES, molecular formula, MW, bioavailability score, Lipinski violations, DL, and toxicity predictions (hepatotoxicity, immunotoxicity, mutagenicity, and carcinogenicity), all of which were inactive with probabilities ranging from 0.62 to 0.93. The boiled egg model for these four compounds was generated using SwissADME and shown as Figure 1A.

Summarises properties of four *Euphorbia hirta* phytochemicals (Pinocembrin, Naringenin, Catechin, Pelargonidin) selected from 207 compounds based on bioavailability (≥30%), drug-likeness (≥0.18), Lipinski's rule, and molecular weight (200-500 Da). Includes SMILES, formula, molecular weight, bioavailability, Lipinski violations, drug-likeness, and inactive toxicity predictions (probability: 0.62-0.93).

Table 1: Properties of Screened Phytochemicals

Name	*Pinocembrin*	*Naringenin*	*Catechin*	*Pelargonidin*
Canonical SMILES	"Oc1cc2O[C@@H](CC(=O)c2c(c1)O)c1ccccc1"	"Oc1ccc(cc1)[C@@H]1CC(=O)c2c(O1)cc(cc2O)O"	"Oc1cc2O[C@H](Cc2c(c1)O)O"	"Oc1ccc(cc1)c1[o+]c2cc(O)cc(c2cc1O)O"
Formula	$C_{15}H_{12}O_4$	C15H12O5	C15H14O6	C15H11O5+
MW	256.25	272.25	290.27	271.24
Bioavailability Score	0.55	0.55	0.55	0.55
Lipinski #violations	0	0	0	0
DL	0.25	0.82	0.64	0.51
Toxicity: Prediction	Inactive: Hept., Immuno., Muta., and Carcino.	Inactive: Hept., Immuno., Muta., and Carcino.	Inactive: Hept., Immuno., Muta., and Carcino.	Inactive: Hept., Immuno., Muta., and Carcino.
Toxicity: Probability	0.67	0.62	0.93	0.83

Target Identification and Overlap Analysis

Using SuperPred, 304 plant-associated targets were identified for the four phytochemicals. For lung cancer, 50,000 targets were retrieved from the GeneCards database, and after filtering for a GIFtS score e" 60 percent, 1,233 targets remained. Intersection analysis using Venny 2.0 revealed 82 common genes between *E. hirta* phytochemical targets and lung cancer-related targets, indicating potential therapeutic relevance (Fig. 1B).

Protein-Protein Interaction (PPI) Network Analysis

The 82 overlapping genes were submitted to the STRING database, generating a PPI network with 82 nodes, 254 edges, an average node degree of 6.2, and an average local clustering coefficient of 0.581. The expected number of edges was 87, with a PPI enrichment p-value <1.0e-16 at a confidence score ≥ 0.7 (Fig. 2A). The network was visualised in Cytoscape (version 3.9.1), and unconnected nodes were removed (Fig. 2B). Using the CytoHubba plugin's degree method, the top 10 hub genes were identified, namely, TP53 (score: 19), SRC (15), EGFR (11), AKT1 (10), MAPK1 (10),

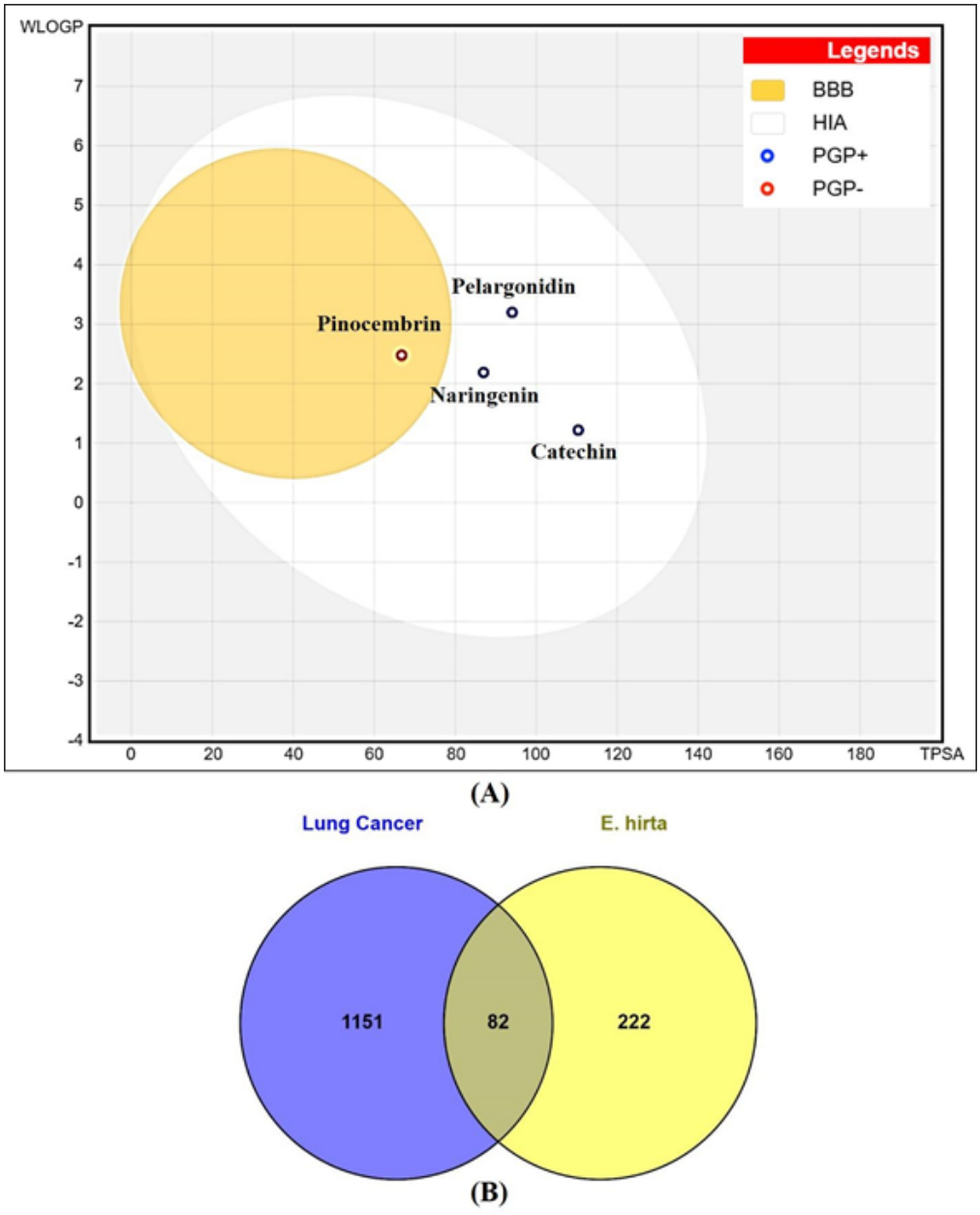

Fig. 1. (A) Bioled egg model: representing different physiochemical properties of Pinocembrin, Naringenin, Catechin, and Pelargonidin
(B) Venn Diagram of Target Gene Overlap: This Venn diagram, generated using Venny 2.0, illustrates the overlap between 304 *E. hirta* phytochemical-associated targets (from SuperPred) and 1,233 lung cancer-related targets (from GeneCards, filtered for GIFtS score ≥ 60%). The intersection reveals 82 common genes, highlighting potential therapeutic targets for *E. hirta* in lung cancer treatment

PTK2 (9), HIF1A (8), IGF1R (7), SMAD3 (6), and STAT1 (6) (Fig. 2C and Table 2). Additional analyses of closeness and Maximal Clique Centrality (MCC) confirmed the significance of these hub genes (Table 2).

GO and KEGG Pathway Analysis

The GO analysis of the hub genes using ShinyGO revealed significant enrichment in BP, CC, and MF. Key BP terms included protein autophosphorylation (enrichment: 20.25, p-value: 1.38E-19), transmembrane receptor protein tyrosine kinase signalling (10.26, 7.09E-19), and regulation of apoptotic processes (5.76, 9.40E-19). CC terms included insulin receptor complex (105.02, 0.0025), membrane raft (8.95, 1.19E-08), and receptor complex (8.81, 4.74E-10). MF terms included transmembrane receptor protein tyrosine kinase activity (37.37, 2.26E-14) and protein kinase activity (9.99, 2.65E-19) (Fig. 3). KEGG pathway analysis identified significant enrichment in pathways such as pathways in Cancer, EGFR Tyrosine Kinase Inhibitor Resistance, HIF-1 Signalling, Focal Adhesion, MAPK Signalling, Akt Signalling, and Ras Signalling, highlighting their relevance to lung cancer progression and treatment (Fig. 4).

Network Visualisation

A comprehensive network integrating *E. hirta*, its phytochemicals, targets, and enriched pathways was constructed using Cytoscape. The network illustrated the relationships between the four phytochemicals, the 82 overlapping targets, and the significant KEGG pathways, providing a holistic view of the potential therapeutic mechanisms of *E. hirta* against lung cancer (Fig. 5).

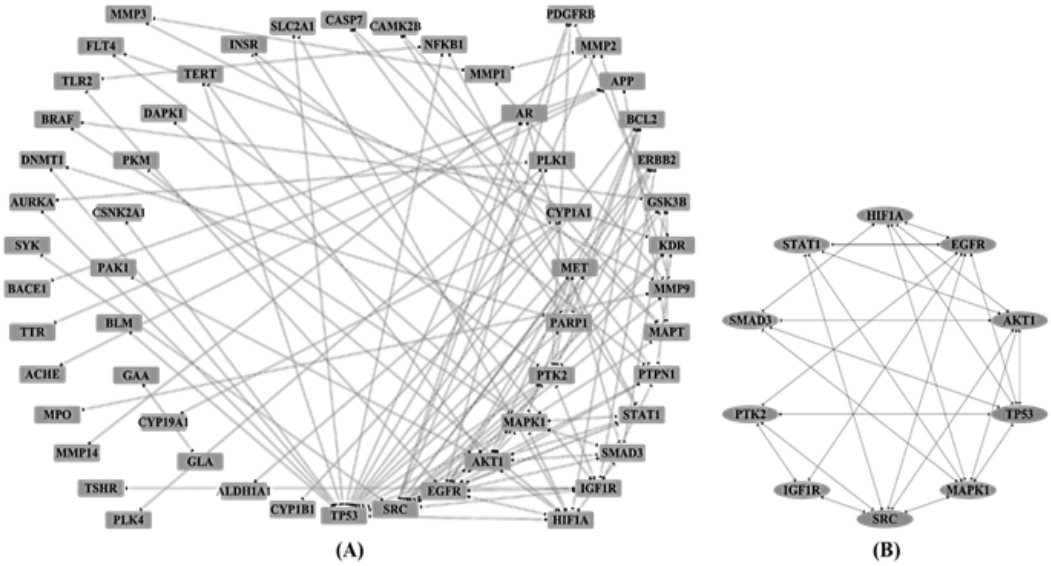

This Figure depicts the PPI network of 82 overlapping genes constructed using the STRING database, featuring 82 nodes, 254 edges, an average node degree of 6.2, and a clustering coefficient of 0.581. With an expected 87 edges and a PPI enrichment p-value < 1.0e-16 (confidence score ≥ 0.7), the network underscores significant interactions among *E. hirta* and lung cancer-related targets

(B) Cytoscape visualization of PPI network: This Figure shows the PPI network of 82 overlapping genes visualized in Cytoscape (version 3.9.1) after removing unconnected nodes. The network highlights the connectivity and interactions among the genes, emphasizing their relevance to *E. hirta*'s potential therapeutic mechanisms in lung cancer

(C) Hub genes identified by CytoHubba: This Figure illustrates the top 10 hub genes (for example, TP53, SRC, EGFR) identified using the CytoHubba plugin's degree method in Cytoscape, with node sizes and colors representing degree scores (for example, TP53: 19; SRC: 15). The visualization highlights the most central genes in the PPI network, critical for *E. hirta*'s anti-lung cancer effects

Table 2: Hub genes by network analysis methods

Rank	*Degree method*		*MCC method*		*Closeness method*	
	Name	*Score*	*Name*	*Score*	*Name*	*Score*
1.	TP53	19	TP53	77	TP53	31.08333
2.	SRC15	SRC	68	SRC	29.33333	
3.	EGFR	11	AKT1	63	MAPK1	27.5
4.	AKT1	10	EGFR	59	EGFR	27.18333
5.	MAPK1	10	MAPK1	57	AKT1	26.91667
6.	PTK2	9	HIF1A	53	PTK2	25.85
7.	HIF1A	8	PTK2	50	HIF1A	24.91667
8.	IGF1R	7	IGF1R	33	ERBB2	23.85
9.	SMAD3	6	SMAD3	32	STAT1	23.66667
10.	STAT1	6	ERBB2	30	SMAD3	22.91667

Differential Expression

The GEPIA2 analysis results for the top three hub genes (TP53, SRC, and EGFR) in A549 cells treated with Euphorbia hirta extract were visualised as box plots for LUAD, n=483 and LUSC, n=338. These box plots illustrate the distribution of mRNA expression levels, with the box representing the interquartile range (IQR, middle 50% of data), whiskers indicating the data range, and outliers (data

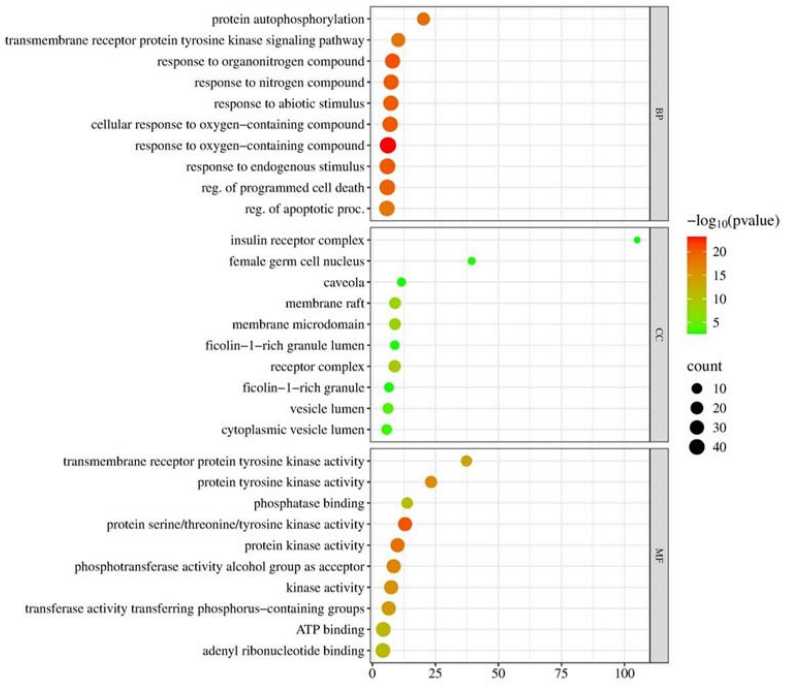

Fig. 3. Gene Ontology (GO) enrichment analysis
This Figure presents the GO enrichment analysis of hub genes using ShinyGO, displaying significant terms for biological processes (for example, protein autophosphorylation, p=1.38E-19), cellular components (for example, insulin receptor complex, p=0.0025), and molecular functions (for example, protein tyrosine kinase activity, p=2.26E-14). Bar or bubble plots visualize enrichment scores and p-values, illustrating functional roles in lung cancer pathways

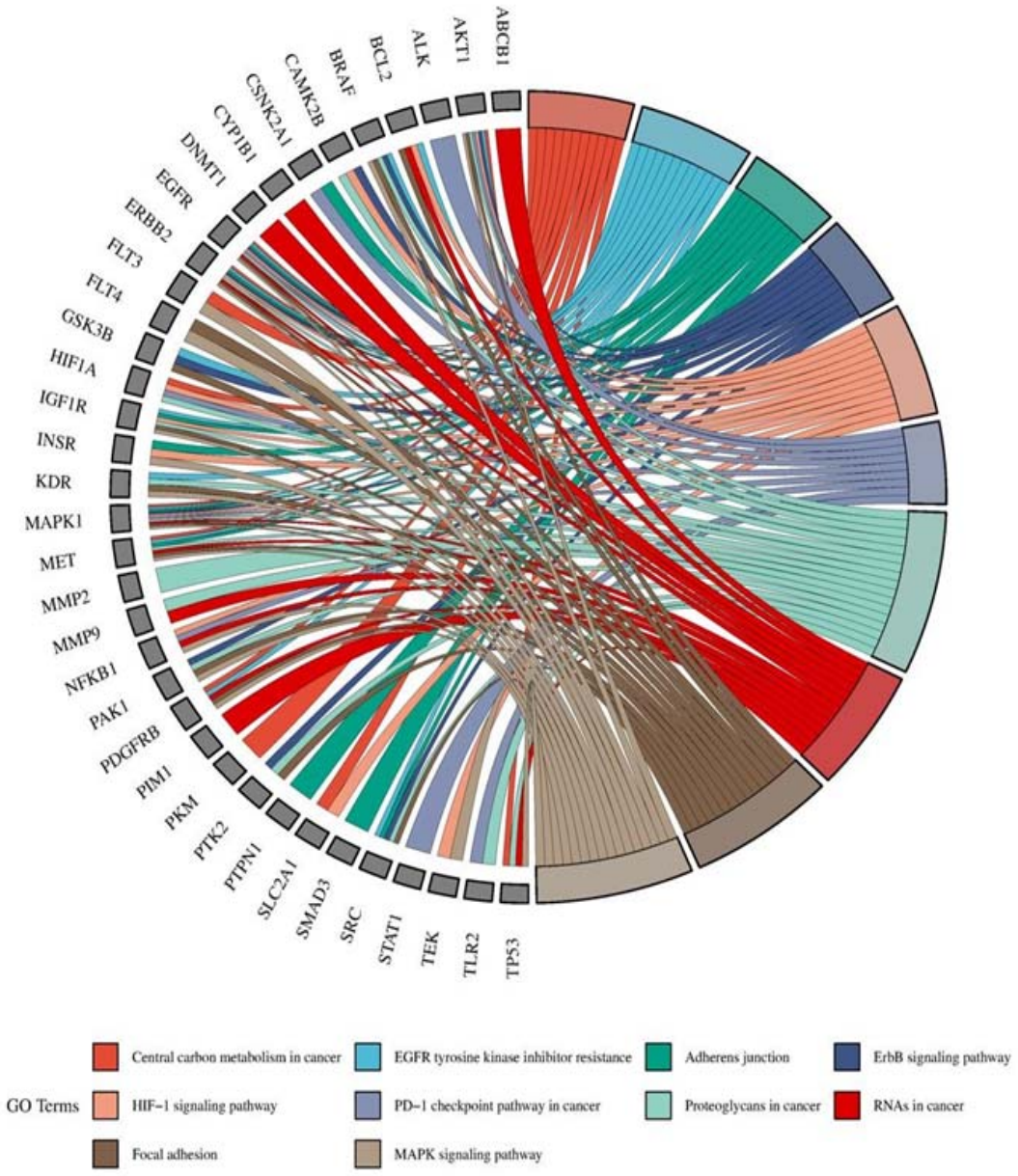

Fig. 4. KEGG pathway enrichment analysis
This Figure shows the KEGG pathway enrichment analysis of hub genes, highlighting significant pathways such as Pathways in Cancer, EGFR Tyrosine Kinase Inhibitor Resistance, HIF-1 Signaling, and MAPK Signaling. The visualization, likely a bar or network plot, displays enrichment scores and p-values, emphasizing pathways relevant to lung cancer progression and *E. hirta*'s therapeutic potential.

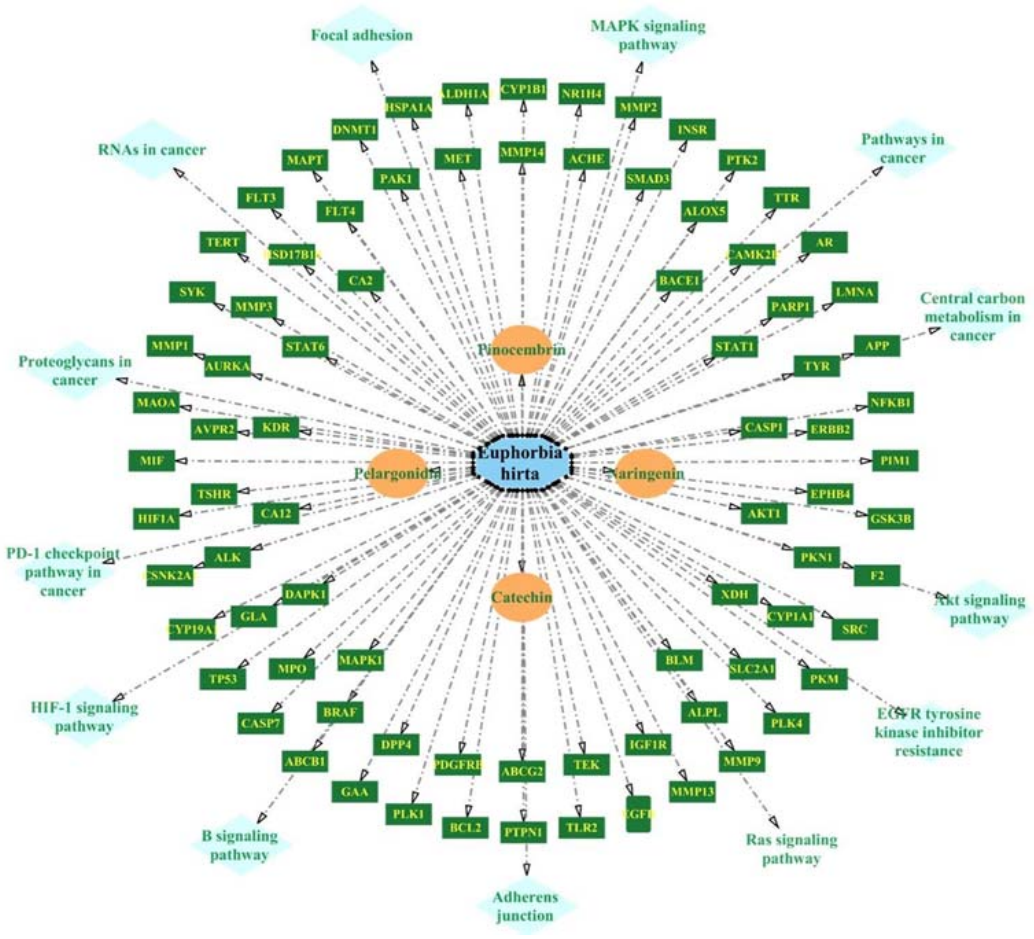

Fig. 5. Comprehensive network of E. hirta, phytochemicals, targets, and pathways
This Cytoscape-generated network integrates *E. hirta*, its four phytochemicals (Pinocembrin, Naringenin, Catechin, Pelargonidin), 82 overlapping target genes, and enriched KEGG pathways. The visualization illustrates the relationships and interactions, providing a holistic view of *E. hirta*'s potential mechanisms in lung cancer treatment

points >1.5 times IQR from the box edges) highlighting extreme expression values. A horizontal line within each box denotes the mean expression level. TP53 exhibited elevated expression in tumour tissues of both LUAD and LUSC, with notably higher levels in LUSC (Fig. 6A). SRC showed increased expression in tumour tissues across both LUAD and LUSC (Fig. 6B). EGFR expression varied between LUAD and LUSC, with comparable levels in LUAD but significantly higher in LUSC tumor tissues (Fig. 6C). These findings highlight distinct expression patterns in LUAD and LUSC, with outliers indicating potential variability in gene expression linked to lung cancer progression and the therapeutic impact of *E. hirta* extract.

Molecular Docking Outcomes

The molecular docking and binding interaction analyses of *E. hirta* phytocompounds with TP53 reveal compound-specific affinities and structural compatibilities, supported by both interaction profiles and docking scores derived from CurPocket cavity predictions (Table 3). Pinocembrin exhibited its best binding affinity in cavity C5 with a Vina score of -6.3 kcal/mol, followed by cavities C4 (-6.2) and C2 (-6.0), indicating moderate binding potential (Fig. 7A). It established conventional hydrogen bonds with SER99 and ARG267, along with Pi-Sigma and Pi-Alkyl interactions involving THR256 and ILE254, respectively. However, an unfavourable donor-donor interaction with ARG267 may impose steric hindrance, weakening its overall stability despite van der Waals support from GLY262 and GLU258. Naringenin displayed a superior docking profile with the best Vina score of -6.6 kcal/mol at cavity C4, followed by C5 (-6.3), indicating strong binding (Fig. 7B). It formed conventional hydrogen bonds with GLY199, SER227, and TYR229, and Pi-Anion interactions with GLU221 and GLU224, supported by van der Waals stabilisation and minimal steric hindrance, suggesting a highly stable and favourable binding conformation. Catechin also demonstrated strong docking affinity, scoring -6.5 kcal/mol in both C4 and C5, with notable hydrogen bonding to GLY199 and Pi-Anion interactions with GLU221 and GLU224 (Fig. 7C). However, an unfavourable donor-donor clash with ASN200 slightly compromises its binding stability, despite favourable van der Waals interactions from multiple residues such as PRO222, THR230, and TYR229. Pelargonidin, while display-

Table 3: Molecular docking with TP53

CurPocket ID	*Vina score*	*Cavity volume (Å³)*	*Centre (x, y, z)*	*Docking size (x, y, z)*
Pinocembrin to TP53				
C5	-6.3	104	-17, -19, 8	20, 20, 20
C4	-6.2	116	-28, -4, -1	20, 20, 20
C2	-6.0	151	-20, 9, 7	20, 20, 20
C1	-5.2	170	-33, -8, 9	20, 20, 20
C3	-5.0	121	-15, 1, 21	20, 20, 20
Naringenin to TP53				
C4	-6.6	116	-28, -4, -1	21, 21, 21
C5	-6.3	104	-17, -19, 8	21, 21, 21
C2	-5.9	151	-20, 9, 7	21, 21, 21
C1	-5.3	170	-33, -8, 9	21, 21, 21
C3	-5.2	121	-15, 1, 21	21, 21, 21
Catechin to TP53				
C4	-6.5	116	-28, -4, -1	21, 21, 21
C5	-6.5	104	-17, -19, 8	21, 21, 21
C2	-6.0	151	-20, 9, 7	21, 21, 21
C1	-5.6	170	-33, -8, 9	21, 21, 21
C3	-5.4	121	-15, 1, 21	21, 21, 21
Pelargonidin to TP53				
C4	-6.3	116	-28, -4, -1	21, 21, 21
C5	-6.2	104	-17, -19, 8	21, 21, 21
C2	-5.7	151	-20, 9, 7	21, 21, 21
C1	-5.4	170	-33, -8, 9	21, 21, 21
C3	-5.3	121	-15, 1, 21	21, 21, 21

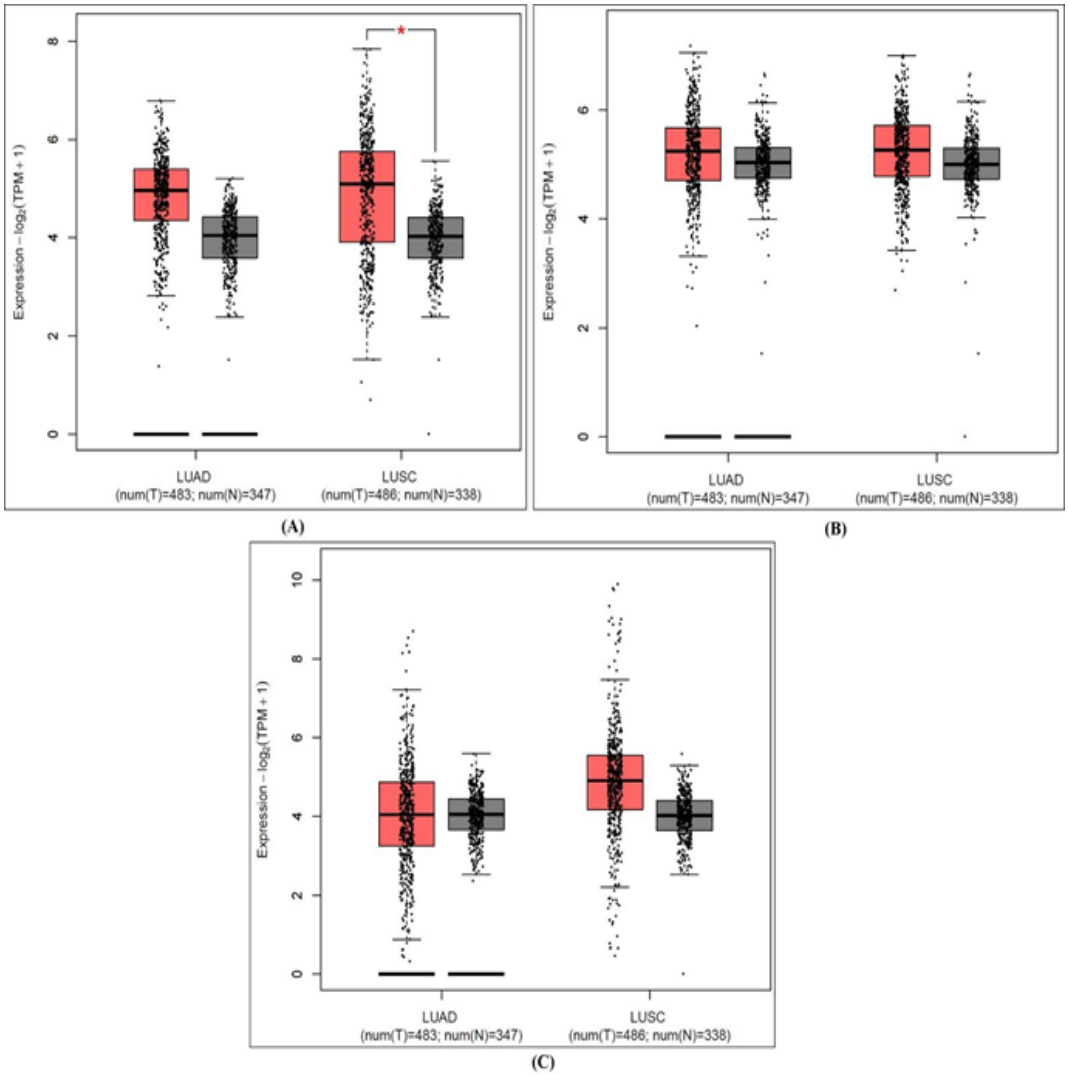

Fig. 6. (A) TP53 expression in LUAD and LUSC (GEPIA2)
This box plot, generated using GEPIA2, shows TP53 mRNA expression in lung adenocarcinoma (LUAD, n=483) and lung squamous cell carcinoma (LUSC, n=338) tumor tissues. The plot displays the interquartile range (IQR), mean (horizontal line), whiskers (data range), and outliers (>1.5× IQR), with higher expression in LUSC, indicating differential expression patterns
(B) SRC Expression in LUAD and LUSC (GEPIA2)
This GEPIA2 box plot illustrates SRC mRNA expression in LUAD (n=483) and LUSC (n=338) tumor tissues, showing elevated expression in both. The plot includes the IQR, mean, whiskers, and outliers, highlighting SRC's consistent overexpression and potential role in lung cancer progression
(C) EGFR Expression in LUAD and LUSC (GEPIA2)
This GEPIA2 box plot depicts EGFR mRNA expression in LUAD (n=483) and LUSC (n=338) tumor tissues, with comparable levels in LUAD but significantly higher expression in LUSC. The plot shows the IQR, mean, whiskers, and outliers, suggesting variability in EGFR expression relevant to *E. hirta*'s effects

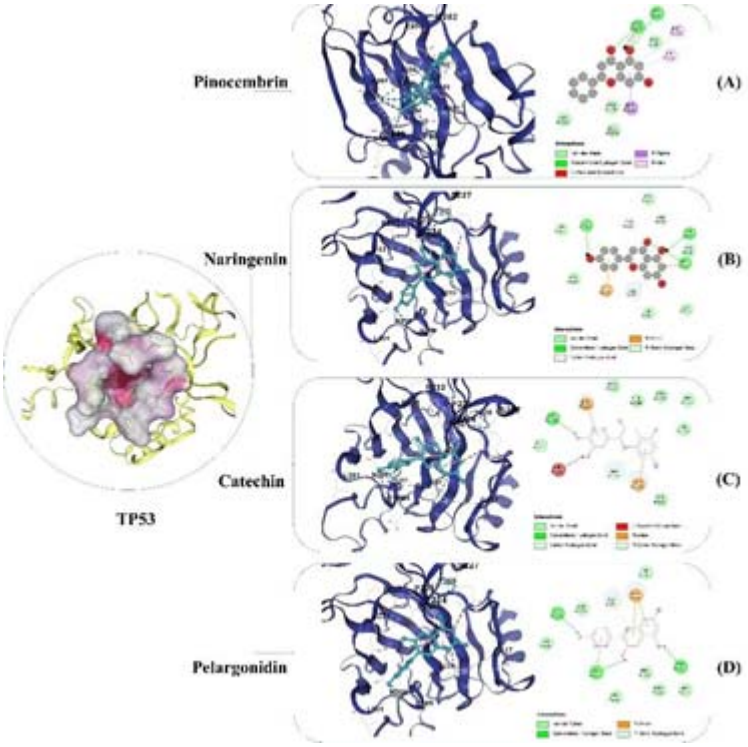

Fig. 7. (A) Molecular docking of pinocembrin with TP53
This Figure visualizes the molecular docking of Pinocembrin with TP53 (PDB ID: 4MZI) at cavity C5 (Vina score: -6.3 kcal/mol), showing hydrogen bonds with SER99 and ARG267, Pi-Sigma/Pi-Alkyl interactions with THR256 and ILE254, and van der Waals interactions. An unfavorable donor-donor interaction with ARG267 is highlighted, indicating moderate binding stability
(B) Molecular docking of naringenin with TP53
This Figure illustrates Naringenin's docking with TP53 at cavity C4 (Vina score: -6.6 kcal/mol), depicting hydrogen bonds with GLY199, SER227, and TYR229, and Pi-Anion interactions with GLU221 and GLU224. The absence of steric hindrance and strong van der Waals stabilization suggest a highly favorable binding conformation
(C) Molecular docking of catechin with TP53
This Figure shows Catechin's docking with TP53 at cavities C4 and C5 (Vina score: -6.5 kcal/mol), with hydrogen bonds to GLY199 and Pi-Anion interactions with GLU221 and GLU224. An unfavorable donor-donor clash with ASN200 is noted, alongside van der Waals interactions from PRO222, THR230, and TYR229, indicating moderate binding stability
(D) Molecular docking of pelargonidin with TP53
This Figure depicts Pelargonidin's docking with TP53 at cavity C4 (Vina score: -6.3 kcal/mol), showing hydrogen bonds with GLY199, TYR229, and GLU221, and a Pi-Anion interaction with GLU224. The absence of unfavorable contacts and extensive van der Waals interactions highlight Pelargonidin's stable and efficient binding to TP53

ing slightly lower docking scores (-6.3 kcal/mol at C4 and -6.2 at C5), demonstrated the most favourable interaction network, forming strong hydrogen bonds with GLY199, TYR229, and GLU221, and a robust Pi-Anion interaction with GLU224, all without any unfavourable contacts (Fig. 7D). The absence of steric clashes, coupled with extensive van der Waals interactions, highlights Pelargonidin as the most stable and efficient TP53 binder, followed closely by Naringenin, with Catechin and Pinocembrin offering moderate yet structurally supportive binding profiles. These results integrate both binding affinity data and detailed residue-level interactions to identify flavonoid-specific TP53 modulatory potential.

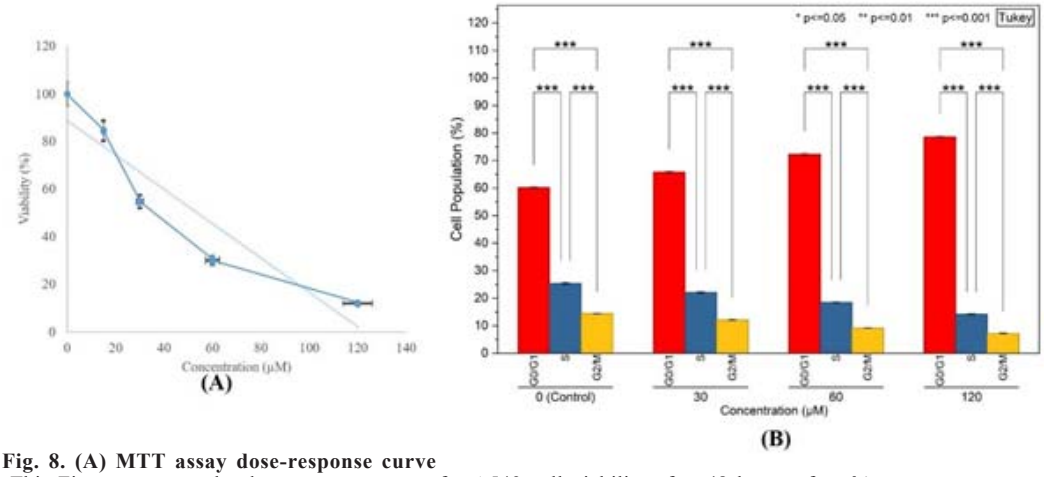

Fig. 8. (A) MTT assay dose-response curve

This Figure presents the dose-response curve for A549 cell viability after 48 hours of *E. hirta* extract treatment at 0, 15, 30, 60, and 120 µM, showing a progressive decrease (100%, 84.6%, 54.8%, 30.2%, 12.2%). The curve, derived from MTT assay data, indicates an IC50 of 26.79 µM, demonstrating moderate cytotoxicity against A549 lung adenocarcinoma cells

(B) Cell cycle distribution analysis

This Figure shows histograms of A549 cell cycle distribution analyzed by flow cytometry after 48 hours of *E. hirta* extract treatment at 0, 30, 60, and 120 µM. The data indicate increased G0/G1 phase arrest (60.2% to 78.6%) and reduced S and G2/M phases, suggesting inhibition of cell cycle progression

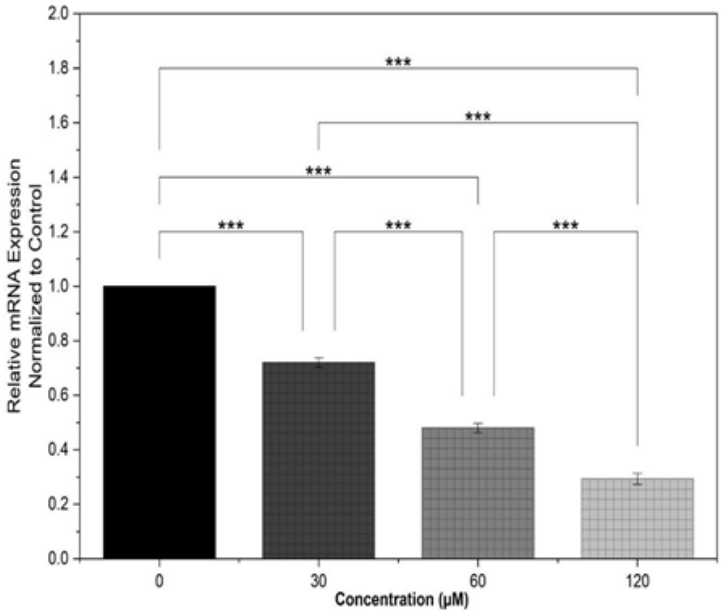

Fig. 9. qRT-PCR analysis of TP53 expression

This Figure displays a bar plot of TP53 mRNA expression in A549 cells treated with *E. hirta* extract at 0, 30, 60, and 120 µM for 48 hours, normalized to GAPDH. Expression levels decrease from 1.0 (control) to 0.72, 0.48, and 0.29, respectively, demonstrating dose-dependent downregulation of TP53 expression, with melting curve analysis confirming amplicon specificity

MTT Assay

The MTT assay revealed that *Euphorbia hirta* ethanolic extract significantly reduced A549 cell viability in a dose-dependent manner. After 48 hours of treatment with 0, 15, 30, 60, and 120 μM concentrations, cell viability decreased progressively, with percentages of 100 percent (control), 84.6 ± 0.40 percent, 54.8 ± 0.35 percent, 30.2 ± 0.65 percent, and 12.2 ± 0.35 percent, respectively (Fig. 8A). The IC50 value, determined from dose-response curves, was calculated as 26.79 μM, indicating moderate cytotoxicity of the extract against A549 lung adenocarcinoma cells.

Cell Cycle Assay

Flow cytometry analysis showed that *E. hirta* extract altered A549 cell cycle distribution. At 0 μM, cells were distributed as 60.2 ± 0.36 percent (G0/G1), 25.4 ± 0.35 percent (S), and 14.4 ± 0.1 percent (G2/M). Treatment with 30, 60, and 120 μM extract increased G0/G1 phase arrest to 65.8 ± 0.36 percent, 72.3 ± 0.44 percent, and 78.6 ± 0.4 percent, respectively, with corresponding reductions in S and G2/M phases, suggesting inhibition of cell cycle progression (Fig. 8B).

mRNA Expression

qRT-PCR analysis demonstrated that *E. hirta* extract downregulated the TP53 (target gene's) mRNA expression in A549 cells. Relative to the untreated control (0 μM, normalised to 1.0), expression levels decreased to 0.72, 0.48, and 0.29 at 30, 60, and 120 μM respectively, after normalisation to GAPDH (Fig. 9). Melting curve analysis confirmed amplicon specificity, indicating that the extract significantly suppresses target gene expression in a dose-dependent manner.

DISCUSSION

The investigation into *Euphorbia hirta*'s therapeutic potential against lung cancer through network pharmacology and in vitro assays provides insights into its modulation of TP53 and associated KEGG pathways, aligning with established literature on lung cancer biology and phytochemical pharmacology. TP53, a pivotal tumour suppressor, is frequently mutated in lung cancers, with mutation rates exceeding 50 percent in NSCLC, particularly in LUSC compared to LUAD. Its role in regulating cell cycle arrest, apoptosis, and DNA repair makes it a central hub in cancer progression. The differential expression of TP53, with higher levels in LUSC, corroborates studies indicating that TP53 mutations or overexpression in LUSC often correlate with aggressive tumour behaviour and resistance to therapies (Canale et al. 2022). This aligns with the present study's findings, where TP53's prominence as a hub gene in the PPI network suggests that *E. hirta*'s phytochemicals, such as Naringenin and Pelargonidin, may target TP53 to modulate lung cancer cell dynamics. The molecular docking profiles, showing strong binding affinities to TP53, particularly for Naringenin (-6.6 kcal/mol), are consistent with reports of flavonoids stabilising p53 protein to enhance apoptosis in cancer cells (Thomas et al. 2022). The absence of steric clashes in Pelargonidin's binding further supports its potential as a stable TP53 modulator, echoing studies where flavonoids like quercetin enhance p53 activity in NSCLC models (Zhou et al. 2023).

The KEGG pathway analysis, highlighting enrichment in pathways in Cancer, EGFR Tyrosine Kinase Inhibitor Resistance, MAPK Signalling, Akt Signalling, and HIF-1 Signalling, underscores the interconnected roles of TP53 and related pathways in lung cancer. The MAPK pathway, critical for cell proliferation and survival, is often dysregulated in lung cancer due to upstream signals from EGFR and SRC, both identified as hub genes in the present study (Zhang et al. 2021). Literature suggests that TP53 interacts with MAPK signalling to regulate cellular responses to stress, with p53-mediated transcription inhibiting MAPK-driven proliferation in NSCLC (Moes-Sosnowska et al. 2024). The study's pathway enrichment aligns with this, suggesting that *E. hirta*'s phytochemicals may suppress MAPK activity via TP53 modulation, potentially counteracting tumour growth. Similarly, the Akt pathway, enriched in the analysis, is a key regulator of cell survival and is frequently activated in lung cancer, particularly in EGFR-mutant tumours (Chen et al. 2022). Studies show that p53 negatively regulates Akt signalling, promoting apoptosis in response to cellular stress (Oršolic and Jembrek 2024). The strong docking affinities of *E. hirta*'s compounds to TP53 suggest a mechanism where these phytochemicals enhance p53's inhibitory effects on Akt, aligning with reports of flavonoid-induced Akt suppression in cancer cells (Liu et al. 2022).

The HIF-1 signalling pathway, also enriched, is relevant in lung cancer's hypoxic tumour microenvironment, where HIF-1α drives angiogenesis and metastasis (Wei et al. 2024). TP53 suppresses HIF-1α activity, and its dysregulation in LUSC correlates with poor prognosis (Zhang et al. 2021). The present study's findings suggest that *E. hirta*'s modulation of TP53 may counteract HIF-1-driven processes, consistent with studies on flavonoids inhibiting HIF-1α in hypoxic cancers (Samec et al. 2021). The EGFR Tyrosine Kinase Inhibitor Resistance pathway highlights a clinical challenge in NSCLC, where TP53 mutations contribute to resistance (Wang and Zhou 2022). The high expression of EGFR in LUSC and its interaction with *E. hirta*'s phytochemicals suggest a potential to overcome resistance, supported by studies where flavonoids sensitise NSCLC cells to EGFR inhibitors (Wang et al. 2021). Collectively, these pathways indicate that *E. hirta*'s phytochemicals target TP53 to influence multiple oncogenic cascades, consistent with its documented anti-cancer, anti-inflammatory, and antioxidant properties in diseases like leukemia and asthma (Samuel et al. 2024; Menon 2021). However, in vivo studies are needed to validate these mechanisms and assess *E. hirta*'s clinical potential in modulating TP53 and KEGG pathways for lung cancer therapy.

CONCLUSION

In conclusion, the network pharmacology and in vitro studies of *Euphorbia hirta* ethanolic extract demonstrate its potent anti-lung cancer activity, mediated by phytochemicals (Pinocembrin, Naringenin, Catechin, Pelargonidin) targeting hub genes TP53, SRC, and EGFR. Molecular docking revealed strong TP53 binding, particularly by Naringenin and Pelargonidin, supporting their role in modulating oncogenic pathways like MAPK, Akt, and HIF-1 signalling. In vitro assays confirmed dose-dependent cytotoxicity (IC50 ≈ 26 μM), G0/G1 phase arrest, apoptosis induction, and TP53 downregulation in A549 cells. These findings highlight *E. hirta*'s therapeutic potential against lung cancer, warranting further in vivo and clinical studies to validate its efficacy and elucidate synergistic mechanisms for targeted cancer therapies.

RECOMMENDATIONS

Based on the conclusions of this study, it is recommended that future research validate the anticancer efficacy of *Euphorbia hirta* and its key phytochemicals through in vivo models and comprehensive pharmacokinetic analyses to establish clinical applicability. Further investigations should also elucidate the precise molecular mechanisms underlying TP53, SRC, and EGFR modulation, particularly their interplay with the MAPK signalling pathway, PI3K/Akt signalling pathway, and HIF-1 signalling pathway. Additionally, exploring synergistic interactions among the identified phytochemicals and with existing chemotherapeutic agents may help develop more effective and targeted therapeutic strategies for lung cancer management.

ACKNOWLEDGMENTS

N/A

DECLARATION OF CONFLICTING INTEREST

Authors declare that they have no conflict of interest to declare.

FUNDING STATEMENT

N/A

ETHICAL APPROVAL AND INFORMED CONSENT STATEMENTS

N/A

DATA AVAILABILITY STATEMENT

The data associated with the paper are not publicly available but are available from the corresponding author on reasonable request.

REFERENCES

Canale M, Andrikou K, Priano I, Cravero P, Pasini L, Urbini M, Delmonte A, Crino L, Bronte G, Ulivi P 2022. The role of TP53 mutations in EGFR-mutated non-small-cell lung cancer: clinical significance and implications for therapy. *Cancers,* 14(5): 1143.

Chen M, Choi S, Wen T, Chen C, Thapa N, Lee JH, Cryns VL, Anderson RA 2022. A p53-phosphoinositide signalosome regulates nuclear AKT activation. *Nature Cell Biology,* 24(7): 1099-1113.

Chen Q, Springer L, Gohlke BO, Goede A, Dunkel M, Abel R, Gallo K, Preissner S, Eckert A, Seshadri L, Preissner R 2021. SuperTCM: A biocultural database combining biological pathways and historical linguistic data of Chinese

materia medica for drug development. *Biomedicine & Pharmacotherapy*, 144: 112315.
Daina A, Michielin O, Zoete V 2017. SwissADME: A free web tool to evaluate pharmacokinetics, drug-likeness and medicinal chemistry friendliness of small molecules. *Scientific Reports,* 7(1): 42717.
Emamzadah S, Tropia L, Vincenti I, Falquet B, Halazonetis TD 2014. Reversal of the DNA-binding-induced loop L1 conformational switch in an engineered human p53 protein. *Journal Of Molecular Biology,* 426(4): 936-944.
Ge SX, Jung D, Yao R 2020. ShinyGO: A graphical gene-set enrichment tool for animals and plants. *Bioinformatics,* 36(8): 2628-2629.
Iskandar B, Lukman A, Syaputra S, Al-Abrori UN, Surboyo MD, Lee CK 2022. Formulation, characteristics and antibacterial effects of Euphorbia hirta L. mouthwash. *Journal of Taibah University Medical Sciences*, 17(2): 271-282.
Jiashuo WU, Zhang F, Zhuangzhuang LI, Weiyi JI, Yue SH 2022. Integration strategy of network pharmacology in Traditional Chinese Medicine: A narrative review. *Journal of Traditional Chinese Medicine,* 42(3): 479.
Khursheed A, Jain V 2022. Euphorbia hirta as a gold mine of high-value phytochemicals: A comprehensive review of its pharmacological activities and possible role against SARS-CoV-2. *Biomedical Research and Therapy,* 9(2): 4930-4949.
Li C, Lei S, Ding L, Xu Y, Wu X, Wang H, Zhang Z, Gao T, Zhang Y, Li L 2023. Global burden and trends of lung cancer incidence and mortality. *Chinese Medical Journal,* 136(13): 1583-1590.
Liu N, Jiang X, Guo L, Zhang C, Jiang M, Sun Z, Zhang Y, Mi W, Li J, Fu Y, Wang F 2022. Mutant p53 achieved Gain-of-Function by promoting tumor growth and immune escape through PHLPP2/AKT/PD-L1 pathway. *International Journal of Biological Sciences*, 18(6): 2419.
Liu Y, Yang X, Gan J, Chen S, Xiao ZX, Cao Y 2022. CB-Dock2: improved protein–ligand blind docking by integrating cavity detection, docking and homologous template fitting. *Nucleic Acids Research*, 50(W1): W159-164.
Menon S 2021. Transcriptomic and metabolic pathway analysis reveals the mutated genes p53 and TP53 and their role in different types of cancer. *International Journal of Engineering Research and Modern Education (IJERME)*, 6(2): 10-33.
Moes-Sosnowska J, Szpechcinski A, Chorostowska-Wynimko J 2024. Clinical significance of TP53 alterations in advanced NSCLC patients treated with EGFR, ALK and ROS1 tyrosine kinase inhibitors: An update. *Tumor Biology,* 46(s1): S309-325.
Oršolic N, Jembrek MJ 2024. Potential strategies for overcoming drug resistance pathways using propolis and its polyphenolic/flavonoid compounds in combination with chemotherapy and radiotherapy. *Nutrients,* 16(21): 3741.
Safran M, Rosen N, Twik M, BarShir R, Stein TI, Dahary D, Fishilevich S, Lancet D 2022. The genecards suite. In: I Abugessaisa, T Kasukawa (Eds.): *Practical Guide To Life Science Databases.* Singapore: Springer Nature Singapore, pp. 27-56.
Samec M, Liskova A, Koklesova L, Mersakova S, Strnadel J, Kajo K, Pec M, Zhai K, Smejkal K, Mirzaei S, Hushmandi K 2021. Flavonoids targeting HIF-1: Implications on cancer metabolism. *Cancers,* 13(1): 130.
Samuel HS, Undie DA, Okibe G, Ochepo OE, Mahmud F, Ilumunter MM 2024. Antioxidant and phytochemical classification of medicinal plants used in the treatment of cancer disease. *Journal of Chemistry Letters,* 5(2): 108-119.
Szklarczyk D, Nastou K, Koutrouli M, Kirsch R, Mehryary F, Hachilif R, Hu D, Peluso ME, Huang Q, Fang T, Doncheva NT 2025. The STRING database in 2025: Protein networks with directionality of regulation. *Nucleic Acids Research,* 53(D1): D730-737.
Tang Z, Kang B, Li C, Chen T, Zhang Z 2019. GEPIA2: An enhanced web server for large-scale expression profiling and interactive analysis. *Nucleic Acids Research,* 47(W1): W556-560.
Thandra KC, Barsouk A, Saginala K, Aluru JS, Barsouk A 2021. Epidemiology of lung cancer. *Contemporary Oncology/Współczesna Onkologia,* 25(1): 45-52.
Thomas AF, Kelly GL, Strasser A 2022. Of the many cellular responses activated by TP53, which ones are critical for tumour suppression? *Cell Death & Differentiation,* 29(5): 961-71.
Tripathi AN, Sati SC, Kumar P 2021. Euphorbia hirta Linnan invasive plant: A review of its traditional uses, phytochemistry and pharmacological properties. *System,* 17: 22.
Vivek-Ananth RP, Mohanraj K, Sahoo AK, Samal A 2023. IMPPAT 2.0: An enhanced and expanded phytochemical atlas of Indian medicinal plants. *ACS Omega,* 8(9): 8827-8845.
Wang F, Zhou Q 2022. The challenges of third-generation EGFR tyrosine kinase inhibitors in the therapy of advanced NSCLC. *Journal of Thoracic Oncology,* 17(4): 481-486.
Wang X, Chen B, Xu D, Li Z, Liu H, Huang Z, Huang K, Lin X, Yao H 2021. Molecular mechanism and pharmacokinetics of flavonoids in the treatment of resistant EGF receptor mutated non small cell lung cancer: A narrative review. *British Journal of Pharmacology*, 178(6):1388-1406.
Wei Z, Li J, Zhong L, Yang D, Li W, Chen W, Zhou H, He Y, Song W, Wang B, Zeng L 2024. DDR1 drives malignant progression of gastric cancer by suppressing HIF 1á ubiquitination and degradation. *Advanced Science,* 11(35): 2308395.
Widyananda MH, Muflikhah L, Ulfa SM, Widodo N 2024. Unveiling the antibreast cancer mechanism of Euphorbia hirta ethanol extract: Computational and experimental study. *Journal of Biologically Active Products from Nature,* 14(3): 359-382.
Xin WA, Zi-Yi WA, Shao LI 2021. TCM network pharmacology: A new trend towards combining computational, experimental and clinical approaches. *Chinese Journal Of Natural Medicines,*19(1): 1.
Zhai Y, Liu L, Zhang F, Chen X, Wang H, Zhou J, Chai K, Liu J, Lei H, Lu P, Guo M 2025. Network pharmacology: A crucial approach in traditional Chinese medicine research. *Chinese Medicine,* 20(1): 8.
Zhang C, Liu J, Wang J, Zhang T, Xu D, Hu W, Feng Z 2021. The interplay between tumor suppressor p53 and hypoxia signaling pathways in cancer. *Frontiers In Cell And Developmental Biology*, 9: 648808.
Zhang X, Xu H, Bi X, Hou G, Liu A, Zhao Y, Wang G, Cao X 2021. Src acts as the target of matrine to inhibit the proliferation of cancer cells by regulating phosphorylation signaling pathways. *Cell Death & Disease,* 12(10): 931.
Zhou B, Yang Y, Pang X, Shi J, Jiang T, Zheng X 2023. Quercetin inhibits DNA damage responses to induce apoptosis via SIRT5/PI3K/AKT pathway in non-small cell lung cancer. *Biomedicine & Pharmacotherapy,* 165: 115071.

Paper received for publication in December, 2025
Paper accepted for publication in April, 2026